Supporting Information

Towards a Quantitative Interfacial Description of Solvation For Li Metal Battery Operation Under Extreme Conditions

John Holoubek[a,*], Kunpeng Yu[a], Junlin Wu[b], Shen Wang[a], Mingqian Li[a], Hongpeng Gao[b], Zeyu Hui[a], Gayea Hyun[a], Yijie Yin[b], Anthony U. Mu[a], Kangwoon Kim[a], Alex Liu[a], Sicen Yu[b], Tod A. Pascal[a,b,c], Ping Liu[a,b,c,*]and Zheng Chen[a,b,c,*]

[a] *Department of NanoEngineering, University of California San Diego, 9500 Gilman Drive, La Jolla, CA, 92093, USA*

[b] *Department of Materials Science, University of California San Diego, 9500 Gilman Drive, La Jolla, CA, 92093, USA*

[c] *Sustainable Power and Energy Center, University of California, San Diego, La Jolla, CA 92093, USA*

Correspondence to:

*(J.H.) E-mail: jholo@stanford.edu

*(Z.C.) E-mail: zhc199@ucsd.edu

*(P.L.) E-mail: piliu@ucsd.edu

Extended Sample Preparation and Characterization Methods

Li metal SEM samples were obtained from Li||Cu coin cells after 10 cycles at room-temperature at 1 mAh cm^{-2} and 0.5 mA cm^{-2} in the plated state. All samples were washed with DME or DEE depending on the applied electrolyte before analysis. All prepared samples were placed in a heat-sealed bag inside the glovebox before they were transferred to the SEM. Cryo-FIB samples were obtained from Li||Cu cells after a 1.8 mAh cm-2 deposition at 0.5 mA cm-2 and -40 ºC or 0.25 mA cm-2 and -60 ºC. Samples were then washed with DME or DEE depending on the applied electrolyte and placed in a heat-sealed bag inside the glovebox before transfer. The cross-section image of samples were prepared under a cryogenic environment (< -150°C) to minimize ion beam damage. During cryogenic etching, a Ga+ ion beam voltage was operated at 30kV at a 15nA milling current. In most cases, a post-etch polishing at 1 nA and the same voltage to better resolve the Li pores.

All XPS measurements were collected with a 0.5 mm × 0.8 mm spot size during acquisition. Survey scans were collected with a 1.0 eV step size, and were followed by high resolution scans with a step size of 0.1 eV for C 1s, O 1s, F 1s, and S2p regions. When applied, etching was carried out with an Ar gas cluster ion source (GCIS) accelerated with 5 keV. Li metal samples were cycled 10 times at their temperature of interest in Li||Cu cells at 0.5 mA cm^{-2} and disassembled in their plated state. All prepared samples were obtained from coin cells and washed with either DME or DEE depending on the applied electrolyte and then placed in a heat-sealed bag inside the glovebox before they were transferred to the XPS. XPS transfer was also conducted in an inert environment.

For NMR, Electrolyte samples were prepared and transferred to sealed NMR tubes in the glovebox before analysis. Temperature control was achieved by cooling Nitrogen gas in Liquid Nitrogen with heater control in the probe from a Varian VT unit. The probe temperature was calibrated against a standard of CH_3OH. Li7 data were acquired at 194.22 MHz with a spectral width of 3884 Hz, with an acquisition time of 4 seconds for 31076 complex points using a 1 second relaxation delay for 16 scans. O17 data were acquired at 67.75 MHz, with a spectral width of 101652 Hz, with an acquisition time of 0.2 seconds for 40660 complex points using a 0.2 second relaxation delay for 6000 scans.

Extended Electrochemical Testing Methods

The ionic conductivity of the electrolyte was measured by a customized two-electrode coin cell, in which the two stainless-steel electrodes are spaced symmetrically between a polytetrafluoroethylene washer with a thickness of 0.027 inches. A glass-fiber separator soaked with electrolyte was housed on the inside of the washer, constraining its surface area to a known value. Measurements were carried out from 40 ºC to -60 ºC in an ESPEC BTX-475 temperature chamber to maintain the cell at a set temperature for 1 hour intervals before each measurement.

Li metal coulombic efficiency (CE) measurements were carried out on Li||Cu cells using the accurate CE determination method.[1,2] Prior to the test, a condition cycle was carried out on all the cells, where 4 mAh cm^{-2} of Li was deposited onto the Cu foil at 0.5 mA cm^{-2}, and then fully stripped to 1 V to form the SEI before CE testing. During testing 4 mAh cm^{-2} was first deposited followed by 10 cycles of 1 mAh cm^{-2} plating and stripping before finally stripping all Li to 1 V. The CE was calculated by dividing the total stripped capacity by the total plated capacity. The cryo-FIB morphological Li studies at various temperatures were conducted in Li||Cu cells plated with 1.8 mAh cm^{-2} and 0.5 mA cm^{-2} at -40 ºC and 1.8 mAh cm^{-2} and 0.25 mA cm^{-2} at -60 ºC.

10 mg cm^{-2} NCA || 20 µm Li coin cells were assembled and subjected to galvanostatic cycling at room temperature, -40 ºC and -60 ºC inside the respective chest freezers after resting for 8 hours to achieve temperature equilibration. For the low temperature tests, a room temperature charge was first carried out at C/10 and transferred to a chamber set at the temperature of interest for cycling. Room temperature cycling consisted of 2 conditioning cycles at C/10 followed by C/3||C/3 or 20 minute charge || C/3 discharge indefinitely. Low temperature cycling was conducted at C/10 for charge, with CC-CV with a C/20 cutoff and C/5 for discharge. The specific capacity basis for C rate determination was 180 mAh g^{-1} with respect to the cathode.

The 10 mg cm^{-2} NCA || 20 µm Li pouch cell were assembled using MTI equipment and the aforementioned NCA and thin Li electrodes. First, an NCA cathodes was cut to 57 x 44 mm using an MTI MSK-180 die cutter and fixed to Al tabs using an MTI MSK-800W ultrasonic welder. The NCA-attached Al tab and a Ni tab were then sealed at a fixed distance along one edge of an MTI Al-laminated pouch cell film and a piece of ~ 60 x 50 mm Celgard 2325 was added to the stack. The partial pouch assembly was then vacuum dried at 80 ºC overnight and transferred to the glovebox, where the 20 µm Li electrode was cut to 58 x 45 mm by hand and affixed to the Ni tab

with MTI strapping tape. The electrical resistance of this contact was found to be negligible when the pouch cell was pressured for cycling. Afterwards, the pouch cell was completely sealed under vacuum in the glovebox using an MTI MSK-115A sealer before a small opening was formed for electrolyte injection. 3 g Ah^{-1} of electrolyte was injected based on the measured LDEE 1-2.6-2 density (1.23 g cm^{-3}), and the pouch was then sealed under ambient pressure to avoid electrolyte loss given the volatility of the applied solvents and the low volume of electrolyte. The mass of the cell before and after injection was measured to ensure an accurate electrolyte loading. The pouch cell was then cycled in a fixed-gap pressurized rig, which is composed of two Al plates bolted together at each corner. Rubber sheets of 1.3 mm thickness cut to slightly larger than the pouch electrodes are placed on either side of the pouch to achieve uniform pressure distribution. The rig was placed under 2800 kPa starting pressure, which is measured with a 1-ton max load cell placed in the pressure stack above the pouch and separated by a smaller Al plate. An elastomer layer to improve pressure distribution homogeneity. We do not explicitly optimize for stack pressure, instead conforming to the optimal value proposed by Wang et al.[3]

For EIS testing, Li||Li cells were assembled with electrolytes of interest and cycled at 10 times at 1 mAh cm^{-2} and 0.5 mA cm^{-2} at room-temperature. Cells were then disassembled in the glovebox, lightly rinsed with DME or DEE depending on their initial electrolyte, and then allowed to dry in the glovebox atmosphere. The cells are then reassembled, either with the same electrolyte that was initially applied during cycling, or with a second electrolyte as described in the main text. Afterwards, EIS is carried out on the reassembled cells from 40 ºC to -60 ºC with a Biologic VSP-300 potentiostat in an ESPEC BTX-475 temperature chamber to maintain the cell at a set temperature for 1 hour intervals before each measurement. DRT fitting is conducted with the DRTtools code (https://sites.google.com/site/drttools/) in MATLAB with Bayesian regression, and Gaussian discretization with 1st-order regularization and a 0.001 regularization parameter. As noted in the main text, we do not consider DRT fitting data produced at low frequencies, which correspond to Warburg diffusion and cannot be properly fit due to the nature of DRT, which inherently assumes an infinite series parallel R-C elements as the equivalent circuit.

Extended Computational Methods

The van der Waals and real space coulomb cutoffs in the MD simulations were 10 Å. A cubic spline was applied to the van der Waals to ensure smooth convergence and vanishing energies and forces at the cutoff (inner cutoff distance of 9Å). The reciprocal space coulomb interactions were computed with a particle-particle-particle-mesh solver,[4] with an error tolerance of 10^{-6}. A total negative charge was applied to one of the two graphene electrodes, with the charge distribution described by Reed et al. via the "fix electrode" command in LAMMPS.[5] Overall neutrality was maintained by adding 5 additional Li^+ atoms, where the second sheet of graphene is kept at 0 charge, and is included only to prevent electrolyte evaporation and to equilibrate the electrolyte volume (see below).

For each system, an initial energy minimization at 0 K (energy and force tolerances of 10^{-4}) was performed to obtain the ground-state structure. After this, the system was slowly heated from 0 K to room temperature at constant volume over 0.01 ns using a Langevin thermostat, with a damping parameter of 100 ps. The system was then subjected to 5 cycles of quench-annealing dynamics in an attempt to eliminate any meta-stable solvation states, where the temperature was slowly cycled between 298 K and 894 K with a ramp period 0.025 ns followed by 0.1 ns of dynamics at either temperature extreme, for 1.25 ns of total time. After annealing, the bulk and interfacial systems were equilibrated via 2 different methods to achieve an equilibrium density. The bulk electrolytes were treated with a constant temperature, constant pressure (1bar) NPT ensemble for 1.5 ns using the Andersen barostat (pressure relaxation constant of 1 ps). As full periodicity is required for the NPT barostat, we instead applied a uniform force to the neutral graphene sheet of the interfacial cell equivalent to 1 bar, which acted as a piston for liquid density equilibration. This force was applied for 1 ns, which was found to be overly sufficient for density equilibration. Finally, we performed 10 ns of constant volume, constant temperature (NVT) production dynamics. Radial distribution functions and density profiles were obtained using the Visual Molecular Dynamics (VMD) software. Snapshots of the various solvation shells, sampled from the simulation trajectory, were also obtained using VMD. The timestep for all simulations was 1 fs and the system propagated forward in time using the time-reversible measure-preserving Verlet integrators derived by Tuckerman et al.[6]

Table S1. Equilibration MD simulation system parameters

Simulation	# Molecules in box	Equilibrated box dimensions (Å)
LDME 1-1.2-4 (Bulk)	100 Li^+, 100 FSI^-, 120 DME, 400 BTFE	49.57 x 49.57 x 49.57
LDME 1-1.8-4 (Bulk)	100 Li^+, 100 FSI^-, 180 DME, 400 BTFE	50.84 x 50.84 x 50.84
LDEE 1-1.7-2 (Bulk)	100 Li^+, 100 FSI^-, 170 DEE, 200 BTFE	44.72 x 44.72 x 44.72
LDEE 1-2.6-2 (Bulk)	100 Li^+, 100 FSI^-, 260 DEE, 200 BTFE	46.91 x 46.91 x 46.91
LDME 1-1.2-4 (Interface)	192 C (Graphene, 11.6 μC cm^{-2}), 47 Li^+, 42 FSI^-, 50 DME, 168 BTFE	25.53 x 19.65 x 104.0 (z dimension given by graphene separation)
LDME 1-1.8-4 (Interface)	192 C (Graphene, 11.6 μC cm^{-2}), 44 Li^+, 39 FSI^-, 70 DME, 156 BTFE	25.53 x 19.65 x 103.7
LDEE 1-1.7-2 (Interface)	192 C (Graphene, 11.7 μC cm^{-2}), 58 Li^+, 53 FSI^-, 90 DEE, 106 BTFE	25.53 x 19.65 x 95.14
LDEE 1-2.6-2 (Interface)	192 C (Graphene, 11.7 μC cm^{-2}), 51 Li^+, 46 FSI^-, 120 DEE, 92 BTFE	25.53 x 19.65 x 92.61

We performed classical free energy sampling on equilibrated MD cells to evaluate the free energy profiles along the following collective variables (CVs): **1)** The Li^+/solvent coordination number (CN) in the first solvation sphere, **2)** The Li^+/Solvent + FSI^- CN in the first solvation sphere, **3)** The Li^+/Li^+ CN within 10 Angstroms, and **4)** the distance between Li^+ and the graphene plane. Specifically, we use the metadynamics protocol to evaluate the potential of mean force along the collective variables.[7] The simulations were carried out using the Colvars module in LAMMPS.[8]

We use the following definition of CN:

$$\sum_{i=1}^{N} \frac{1-\left(\frac{r_i}{r_0}\right)^p}{1-\left(\frac{r_i}{r_0}\right)^q}$$

where p=6 and q=12. r_i is the distance between Li^+ and the i-th coordinating atom. In this case only the solvent and FSI^- oxygens were considered as coordinating species, as nitrogen was not determined to coordinate directly with Li^+ from equilibration simulations. r_0 is the cut-off radius

that defines atoms as inside or outside of the first solvation sphere, where *i* runs over the range that includes all possible coordinating atoms (e.g., all oxygen atoms in the simulation box). The applied cut-off radius was 3.07 Angstroms, similar to previous work with comparable ether solvents.[9,10]

MD simulation boxes (Table S1) after equilibration (Equilibration MD section) were used as initial configuration for the free energy sampling with the metadynamics protocol. This protocol was applied in either a 1-D or 2-D fashion depending on the purpose of the simulation. Typically, free energy sampling was determined to be converged when both of the following conditions were met: **1)** The phase space of interest for the simulation was entirely explored (i.e., all relevant solvation/electrode distance states were visible in the profile), and **2)** the standard deviation of free energy profiles converge to < 0.5 kCal mol^{-1} within the phase space of interest over the averaged time period (last 100 ns). For LHCE systems, we found that the different sizes of ion aggregates across systems significantly affected the ability of the systems to reach ballistic motion along their respective CVs, which is responsible for criteria #2.

In Table S2 we summarize the parameters of the metadynamics free energy sampling for various simulations: height of the Gaussian hills (kcal/mol), frequency of hill creation (steps), width of hills in Å for electrode distance or unitless for CN, and simulation time in ns. In all cases, "well-tempered" metadynamics was applied with a bias of 10x the simulation temperature.[11] The free energy profiles shown in this work were averaged over the last 100 ns for 298 K simulations, and the last 200 ns for 213 K simulations. 1-D profiles were plotted in Origin Pro, whereas 2-D profiles were plotted in gnuplot. Averaged plots and integrated 1-D slices from the 2-D plots shown in figures 2, 3, and 4 were calculated using Python. The 1-D projection of the Li^+ desolvation path in LDME 1-1.2-4 (Figure S20) was sampled using a rudimentary pathfinding script (Python), which connected local minima within a radius of 0.075 CV units between defined (CN, electrode distance) starting and ending points.

Table S2. Metadynamics parameters for each simulation applied in this work.

Simulation	Hill Height (kCal mol^{-1})	Hill Width (kCal mol^{-1})	Hill Creation Freq. (fs)	Simul. Time (ns)
LDME 1-1.2-4 and 1-1.8-4 Bulk **1-D, 298 K** *Fig. 5b:* Li^+/solvent CN (0 – 6)	0.02	0.02	500	~500
LDME 1-1.2-4 and 1-1.8-4 Bulk **1-D, 298 K** *Fig. S14a:* Li^+/total CN (0 – 6)	0.02	0.02	500	~300
LDME 1-1.2-4 and 1-1.8-4 Bulk **1-D, 298 K** *Fig. S15:* Li^+/self CN (0 – 30)	0.02	0.05	500	~250
LDEE 1-1.7-2 and 1-2.6-2 Bulk **1-D, 298 K** *Fig. 5c:* Li^+/solvent CN (0 – 6)	0.02	0.02	500	~500
LDEE 1-1.7-2 and 1-2.6-2 Bulk **1-D, 298 K** *Fig. S14b:* Li^+/total CN (0 – 6)	0.02	0.02	500	~300

LDEE 1-1.7-2 and 1-2.6-2 Bulk **1-D, 298 K** *Fig. S15:* Li^+/self CN (0 – 30)	0.02	0.05	500	~250
LDME 1-1.2-4 and 1-1.8-4 11.6 µC cm^{-2} graphene **2-D, 298 K** Li^+/electrode distance (1.5-12 Å) Li^+/solvent CN (0 – 6.0) *Figure 5f and 5g*	0.02	0.05	200	~500
LDME 1-1.2-4 and 1-1.8-4 11.6 µC cm^{-2} graphene **2-D, 298 K** Li^+/electrode distance (1.5-12 Å) Li^+/total CN (0 – 6.0) *Figure S20a and S20b*	0.02	0.05	200	~450
LDEE 1-1.7-2 and 1-2.6-2 11.6 µC cm^{-2} graphene **2-D, 298 K** Li^+/electrode distance (1.5-12 Å) Li^+/solvent CN (0 – 6.0) *Figure 5j and 5k*	0.02	0.05	200	~500
LDEE 1-1.7-2 and 1-2.6-2 11.6 µC cm^{-2} graphene **2-D, 298 K** Li^+/electrode distance (1.5-12 Å) Li^+/total CN (0 – 6.0) *Figure S20c and S20d*	0.02	0.05	200	~350

Quantum chemistry simulations were performed using the Q-Chem 5.1 quantum chemistry package. Simulations involved a geometry optimization step at the M06-HF//6-31+G(d,p) level of theory followed by single point energy and harmonic vibrational analysis at the M06-HF//6-311++G** level of theory. The single-solvent binding free energies shown in Figure 1 were calculated as:

$$\Delta G_b = \Delta H_b - T\Delta S_b$$

where

$$\Delta H_b = \left(E_{Li^+ + solv.} + H_{T,Li^+ + solv}\right) - \left(E_{Li^+} + H_{T,Li^+}\right) - \left(E_{solv.} + H_{T,solv}\right)$$

$$\Delta S_b = S_{vib,Li^+ + solv.} - S_{vib,Li^+} - S_{vib,solv.}$$

In this case, E is the total DFT energy, H_T is the thermal enthalpy correction, and S_{vib} is the vibrational entropy of simulations containing (Li^+ + solvent), or each isolated component.

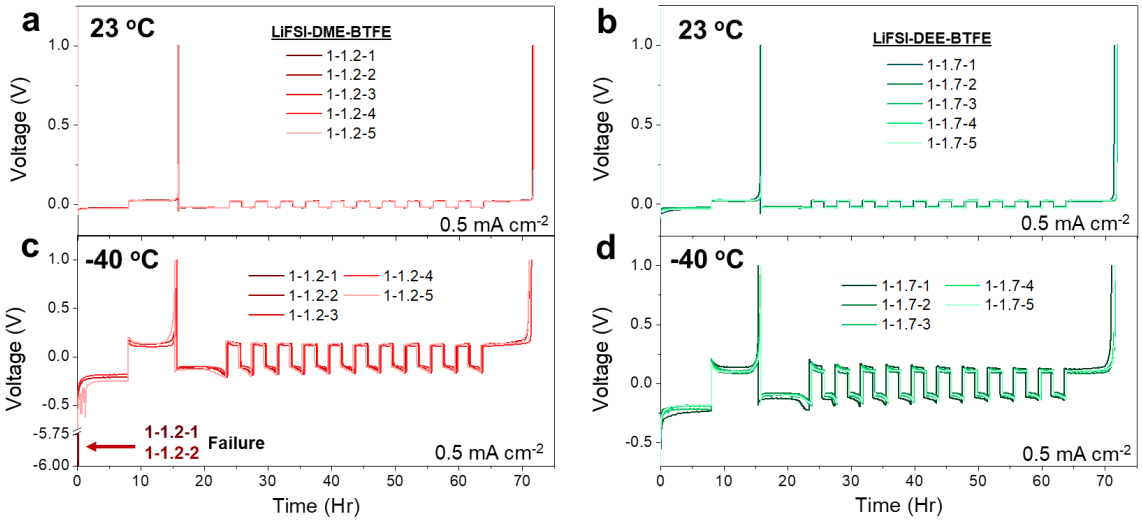

Figure S1. Voltage profiles of Li||Cu Coulombic efficiency measurements in LHCE systems as a function of global dilution. Voltage profiles of **a)** LDME and **b)** LDEE systems at 23 ºC. Voltage profiles of **c)** LDME and **d)** LDEE systems at -40 ºC.

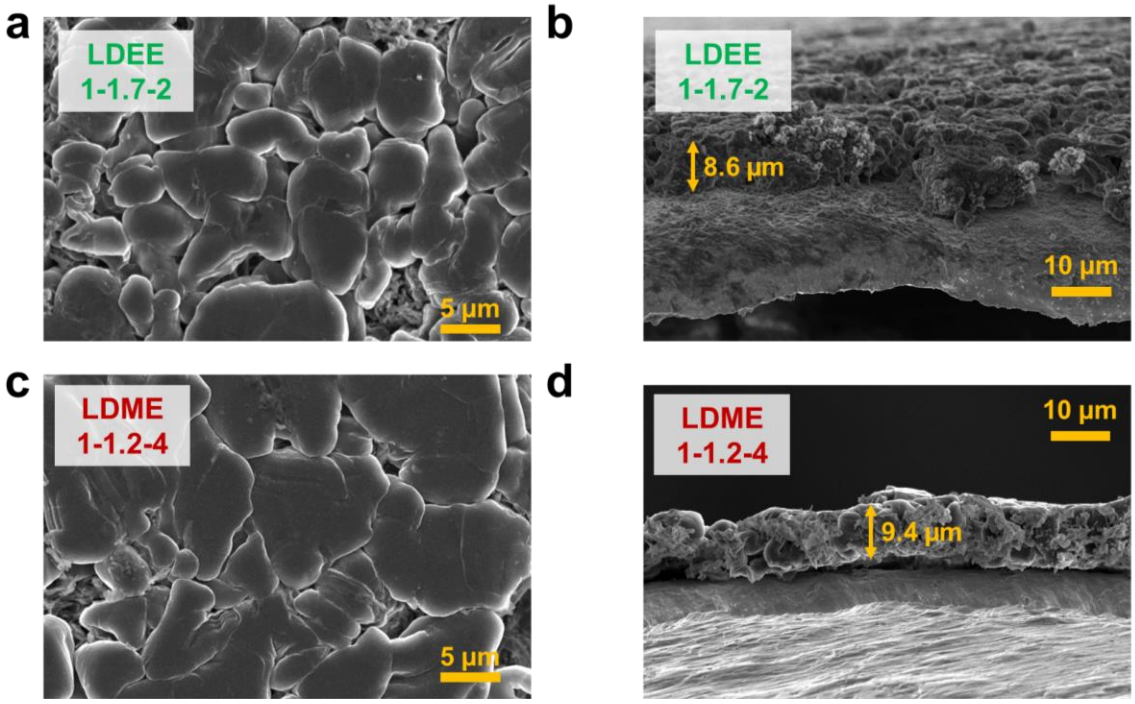

Figure S2. SEM images of 1 mAh cm^{-2} Li metal after 10 cycles at 0.5 mA cm^{-2} and 23 ºC in locally-saturated LHCE systems. **a)** Planar, and **b)** Cross-section images of Li plated in LDEE 1-1.7-2. **c)** Planar, and **d)** Cross-section images of Li plated in LDME 1-1.2-4.

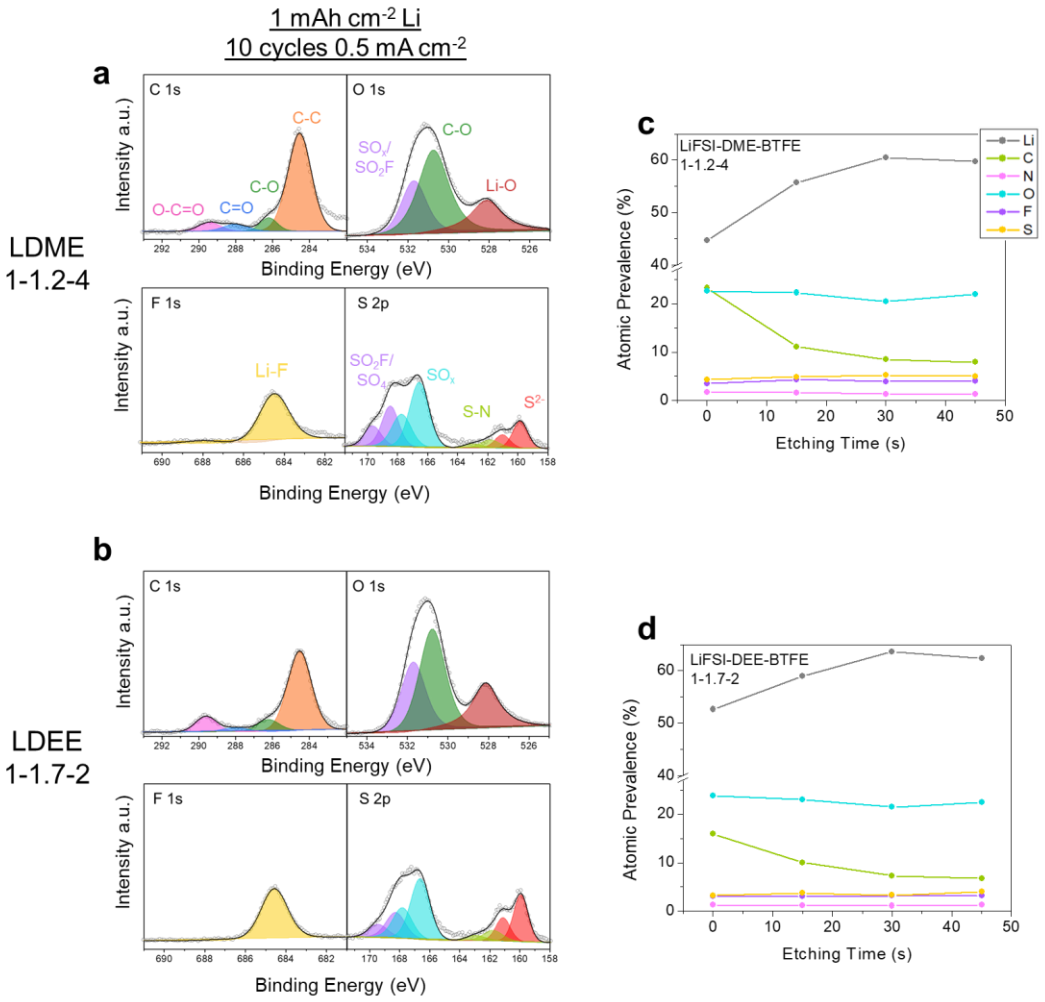

Figure S3. XPS spectra of 1 mAh cm^{-2} Li metal after 10 cycles at 0.5 mA cm^{-2} and 23 ºC in locally-saturated LHCE systems. C1s, O1s, F1s, and S2p detailed spectra of Li cycled in **a)** LDME 1-1.2-4, and **b)** LDEE 1-1.7-2. Atomic prevalence as a function of etching time of Li metal cycled in **c)** LDME 1-1.2-4, and **d)** LDEE 1-1.7-2.

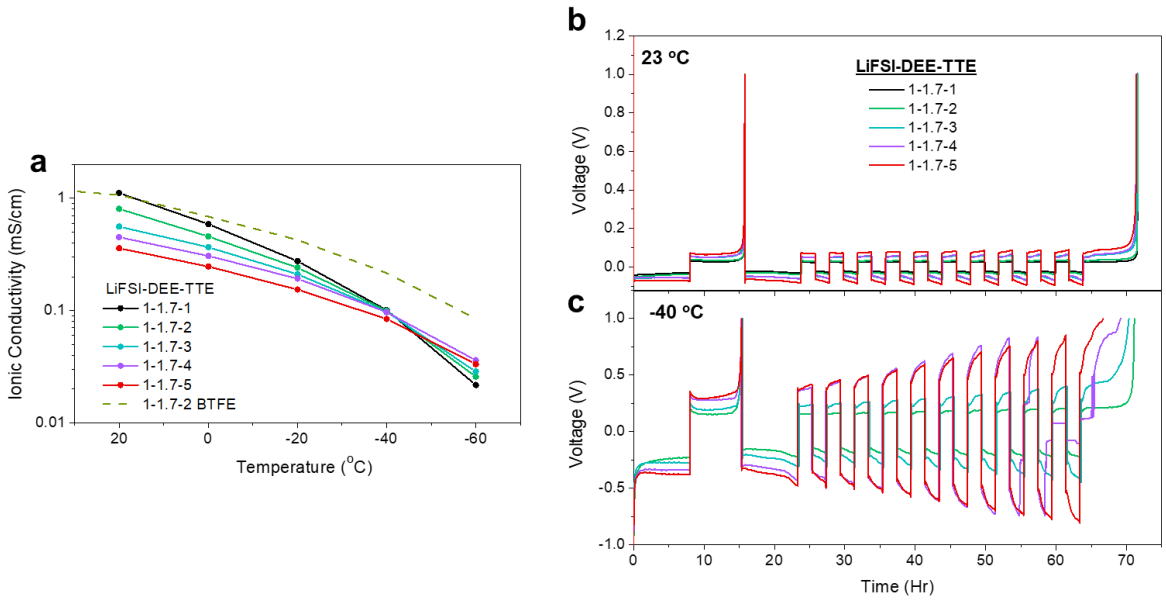

Figure S4. Impact of global dilution on LDEE systems based on the 1,1,2,2-tetrafluoroethyl-2,2,3,3-tetrafluoropropyl ether (TTE) diluent. **a)** Ionic conductivities of TTE-based LDEE systems as a function of TTE composition. Li||Cu CE measurements at 0.5 mA cm^{-2} and **b)** 23 and **c)** -40 °C.

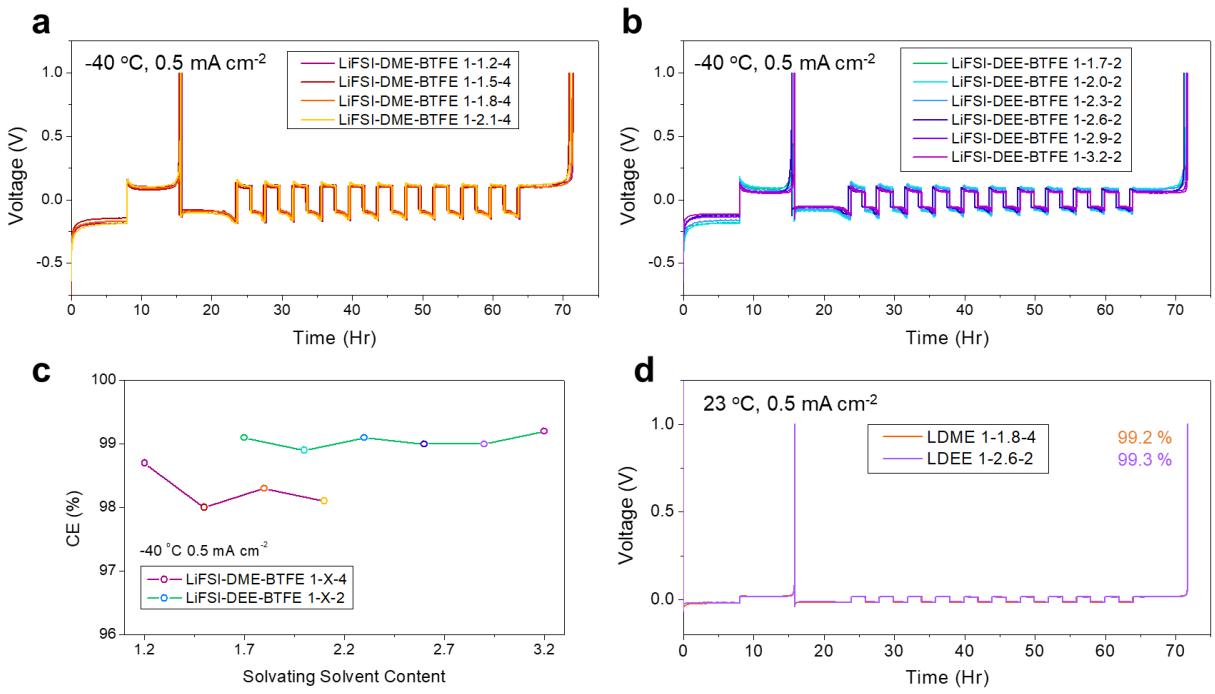

Figure S5. Impact of local dilution Li metal performance. Li||Cu CE measurements at -40 °C and 0.5 mA cm^{-2} in **a)** LDME systems and **b)** LDEE systems. **c)** Summary of measured cycling CE at -40 °C in LDME and LDEE systems as a function of solvating solvent content. **d)** Li||Cu CE measurements at 23 °C and 0.5 mA cm^{-2}.

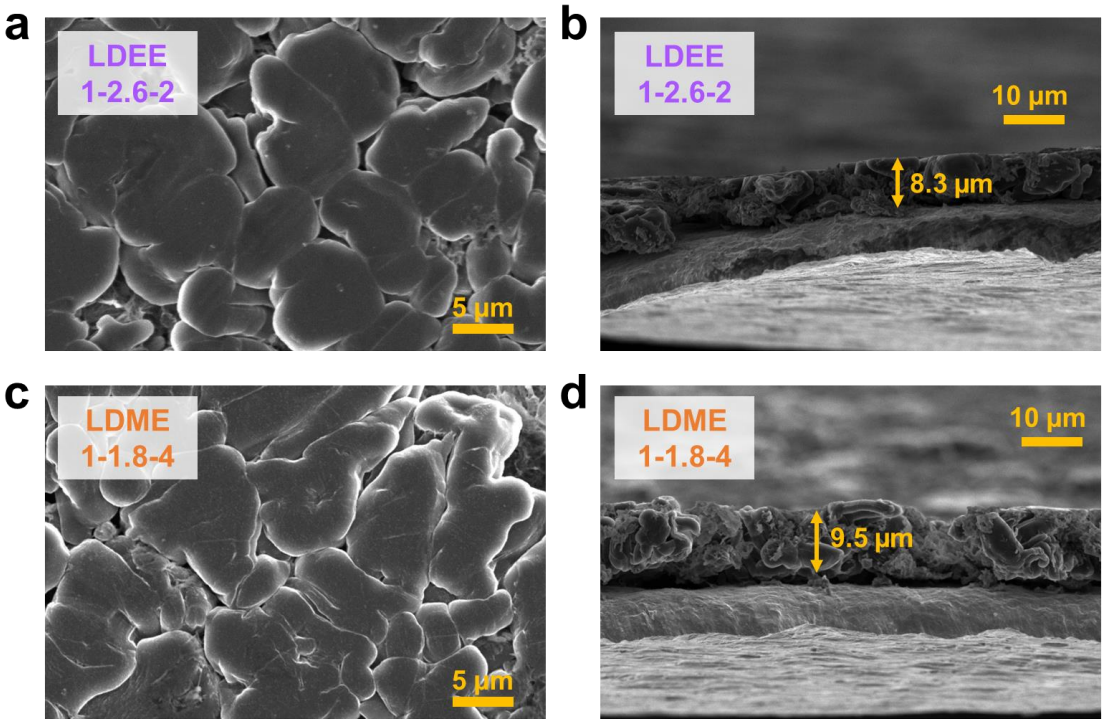

Figure S6. SEM images of 1 mAh cm^{-2} Li metal after 10 cycles at 0.5 mA cm^{-2} and 23 ºC in locally-saturated LHCE systems. **a)** Planar, and **b)** Cross-section images of Li plated in LDEE 1-2.6-2. **c)** Planar, and **d)** Cross-section images of Li plated in LDME 1-1.8-4.

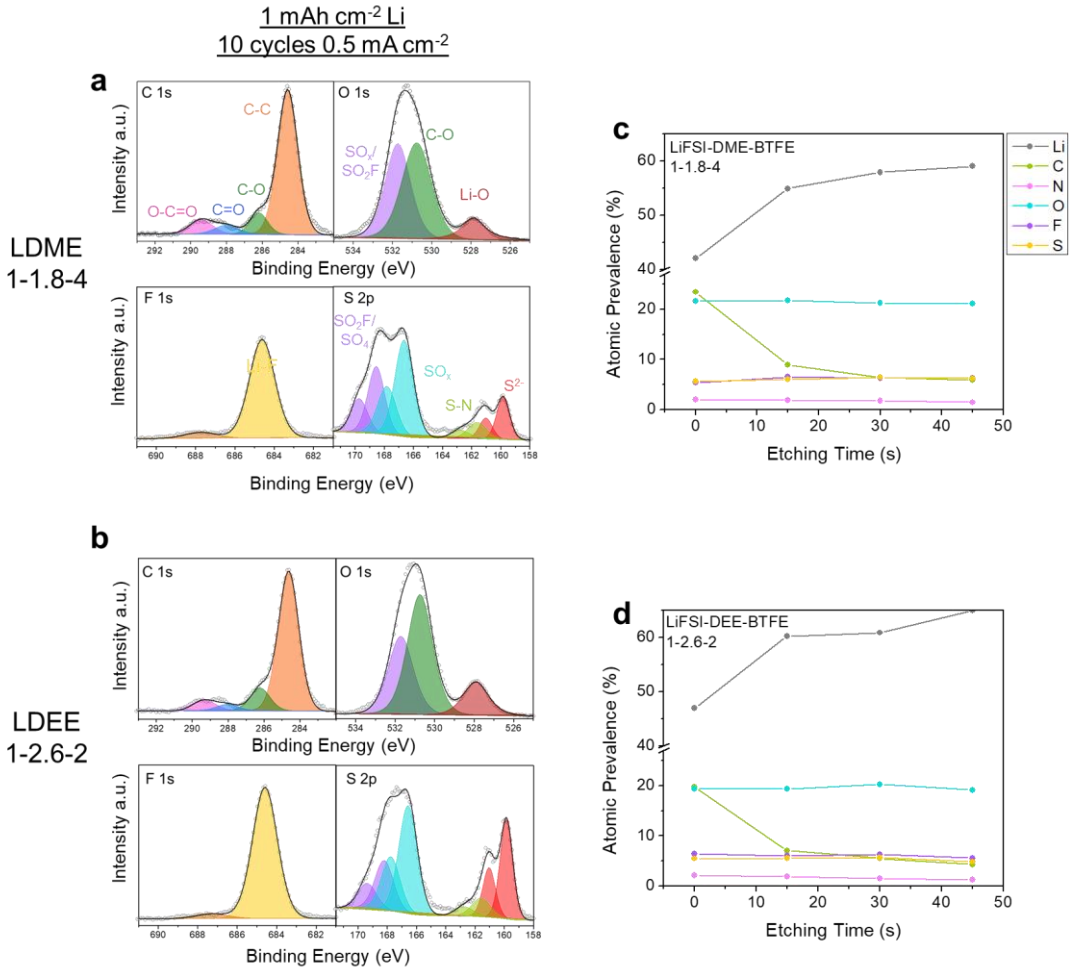

Figure S7. XPS spectra of 1 mAh cm^{-2} Li metal after 10 cycles at 0.5 mA cm^{-2} and 23 ºC in locally-saturated LHCE systems. C1s, O1s, F1s, and S2p detailed spectra of Li cycled in **a)** LDME 1-1.8-4, and **b)** LDEE 1-2.6-2. Atomic prevalence as a function of etching time of Li metal cycled in **c)** LDME 1-1.8-4, and **d)** LDEE 1-2.6-2.

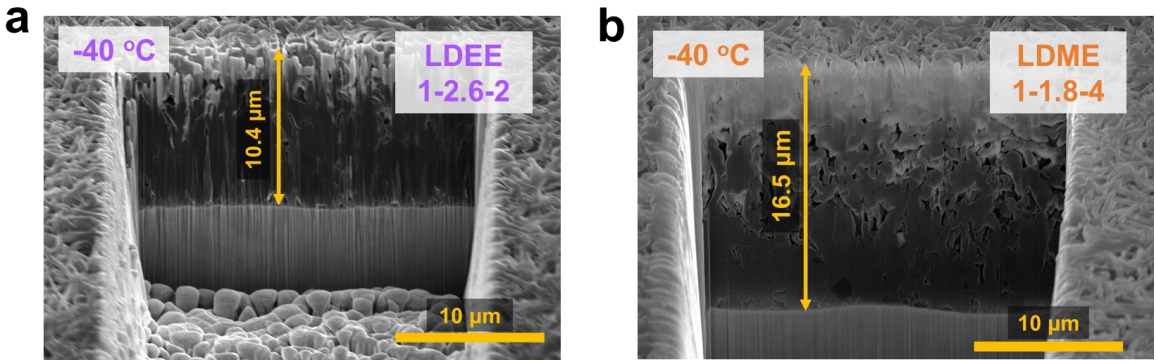

Figure S8. SEM microscopy of 1.8 mAh cm^{-2} Li metal plated at -40 ºC and 0.5 mA cm^{-2} after cryo-FIB milling in **f)** LDME 1.8, and **g)** LDEE 2.6.

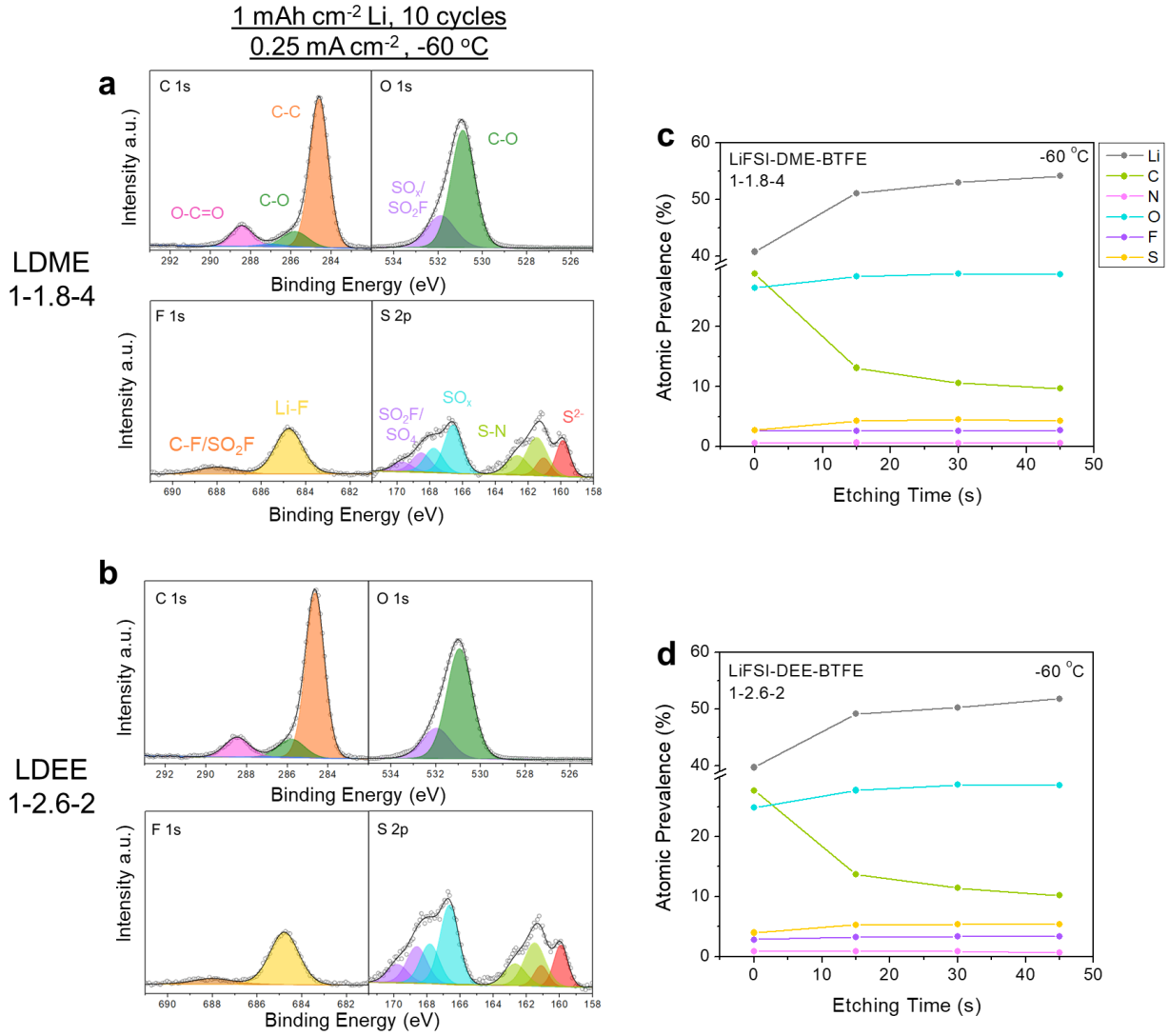

Figure S9. XPS spectra of 1 mAh cm^{-2} Li metal after 10 cycles at 0.25 mA cm^{-2} and -60 ºC in locally-saturated LHCE systems. C1s, O1s, F1s, and S2p detailed spectra of Li cycled in **a)** LDME 1-1.8-4, and **b)** LDEE 1-2.6-2. Atomic prevalence as a function of etching time of Li metal cycled in **c)** LDME 1-1.8-4, and **d)** LDEE 1-2.6-2.

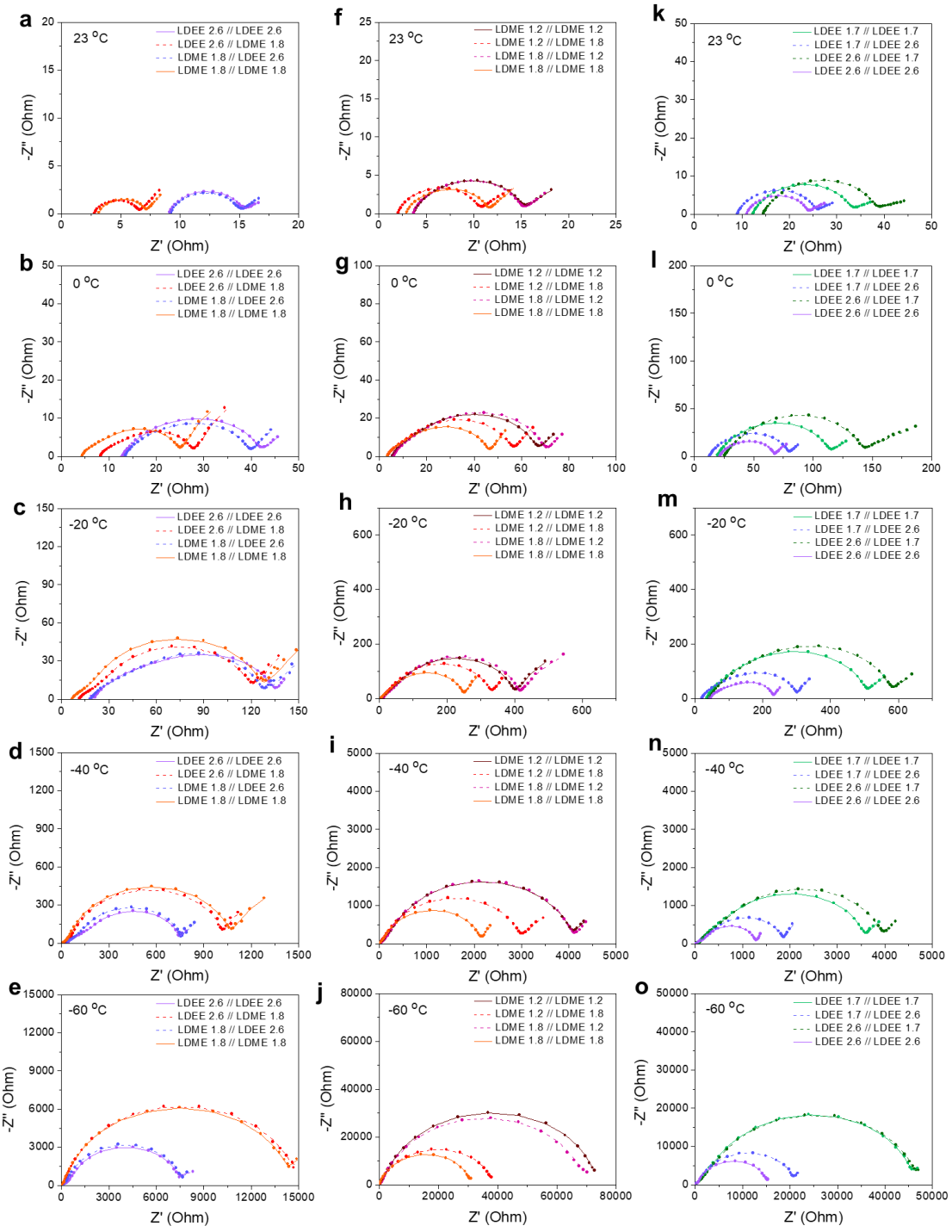

Figure S10. Raw Nyquist plots from DRT profiles shown in Figure 3 and S10. DRT fits are shown with lines. **a-e)** 23 to -60 ºC data for LDEE 1-2.6-2 / LDME 1-1.8-4 matrix. **f-j)** 23 to -60 ºC data for LDME 1-1.2-4 / LDME 1-1.8-4 matrix. **k-o)** 23 - -60 ºC data for LDEE 1-1.7-2 / LDEE 1-2.6-2 matrix. In all cases, DRT fitting after the semi-circle was neglected due to Warburg incompatibility with the technique.

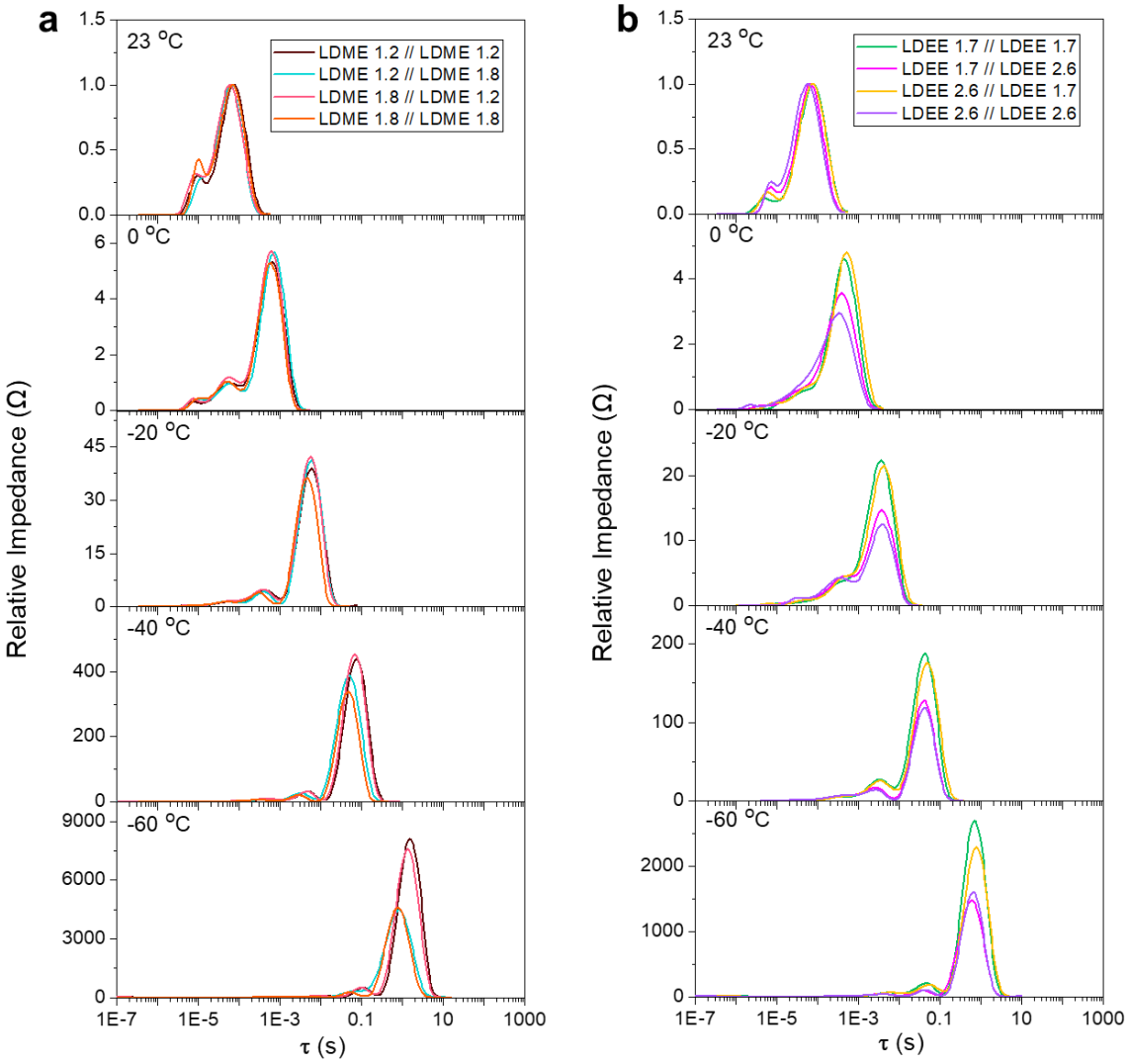

Figure S11. DRT profiles from EIS measurements between 23 and -60 °C of **a)** LDME local dilution series and **b)** LDEE local dilution series. In all cases, DRT fitting after the semi-circle was neglected due to Warburg incompatibility with the technique.

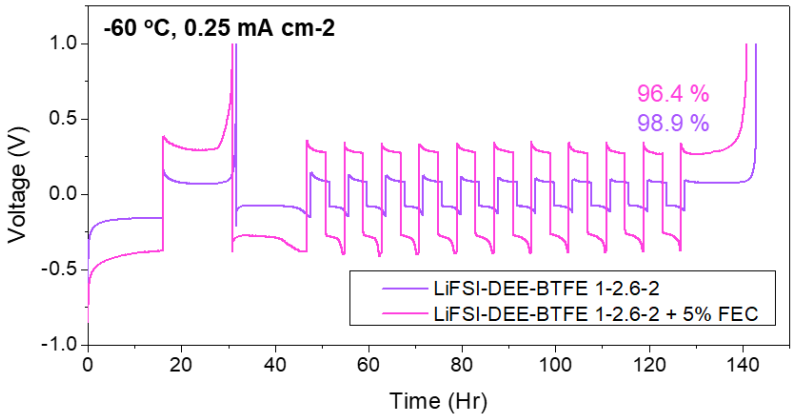

Figure S12. Li||Cu CE measurement of LDEE 1-2.6-2 with a 5% FEC additive.

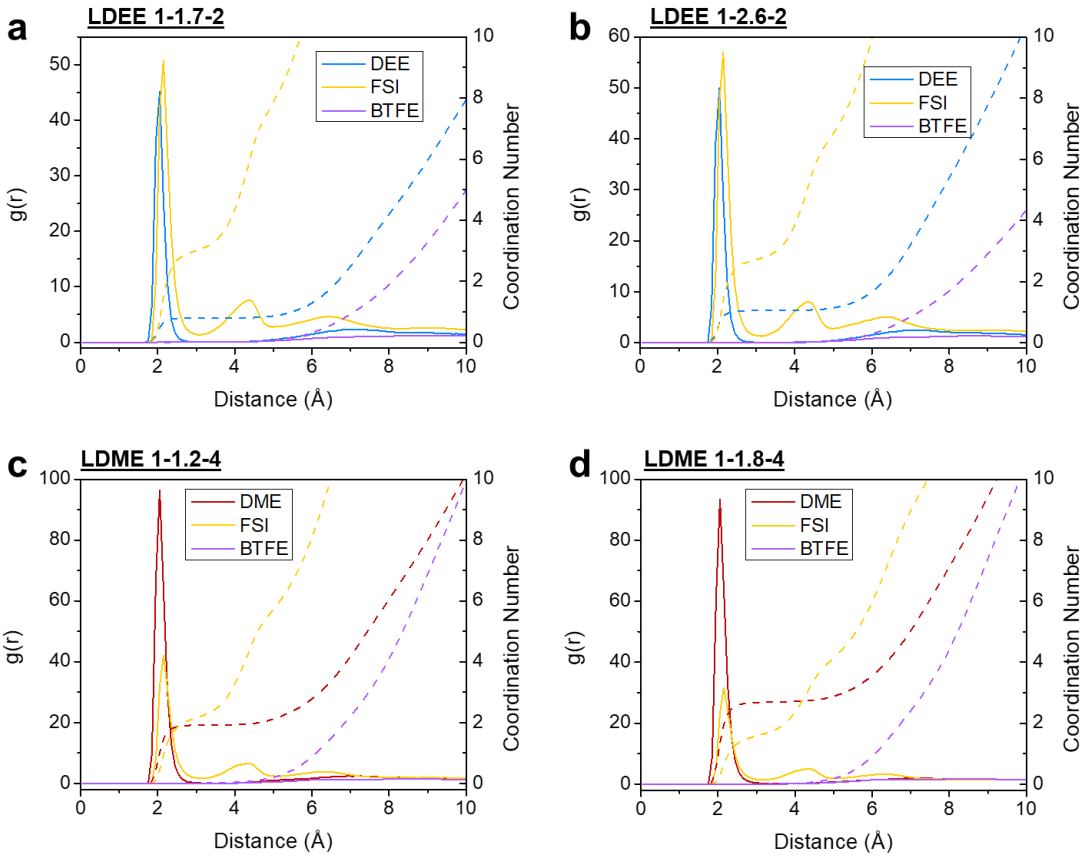

Figure S13. Radial distribution functions (RDF) of various solvating components with respect to Li^+. **a)** LDEE 1-1.7.2, **b)** LDEE 1-2.6-2, **c)** LDME 1-1.2-4, **d)** LDME 1-1.8-4. Only oxygen atoms were considered for solvation. For DME, the CN of the solvent molecules are ½ of the CNs shown above as there are 2 oxygens per molecule.

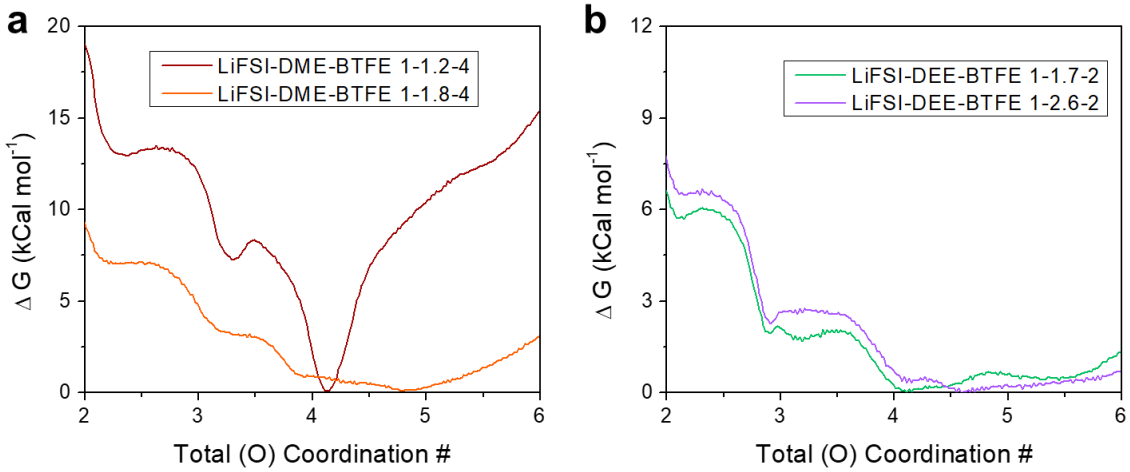

Figure S14. 1-D free energy profiles of LHCE systems with respect to solvating solvent (i.e. DME or DEE) and FSI^- O coordination. **a)** LDME 1-1.2-4 and 1-1.8-4 (Note that DME contains 2 oxygen atoms per molecule). **b)** LDEE 1-1.7-2 and 1-2.6-2.

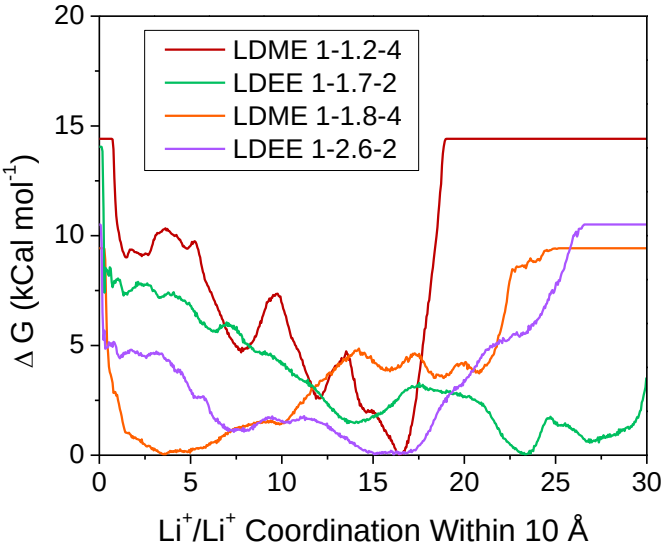

Figure S15. 1-D free energy profiles of LHCE systems with respect to self (Li^+/Li^+) coordination within 10 Angstroms.

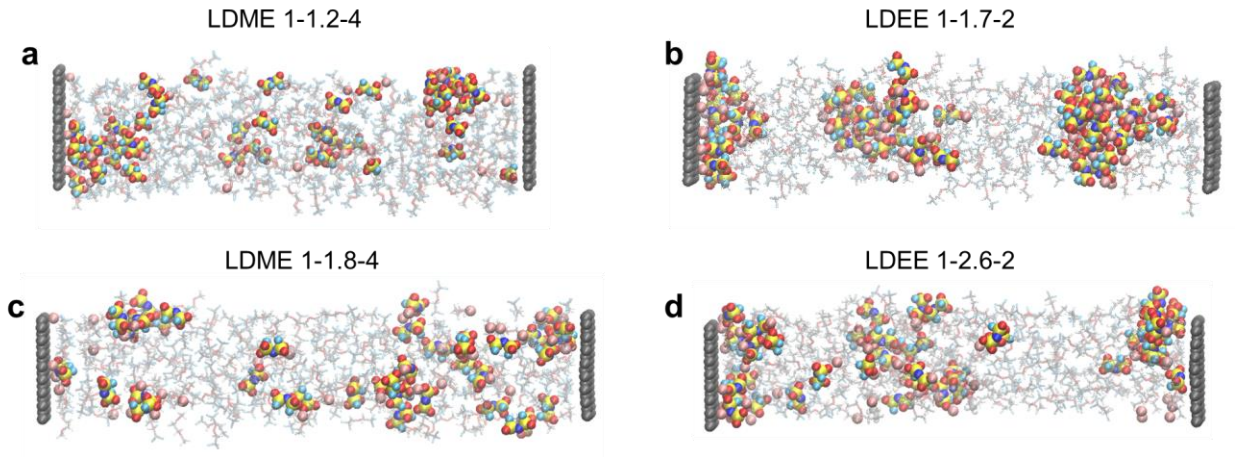

Figure S16. Snapshots of interfacial MD cells demonstrating visual changes in AGG sizes as a function of solvent chemistry and local dilution. **a)** LDME 1-1.2-4, **b)** LDEE 1-1.7-2, **c)** LDME 1-1.8-4, **d)** LDEE 1-2.6-2.

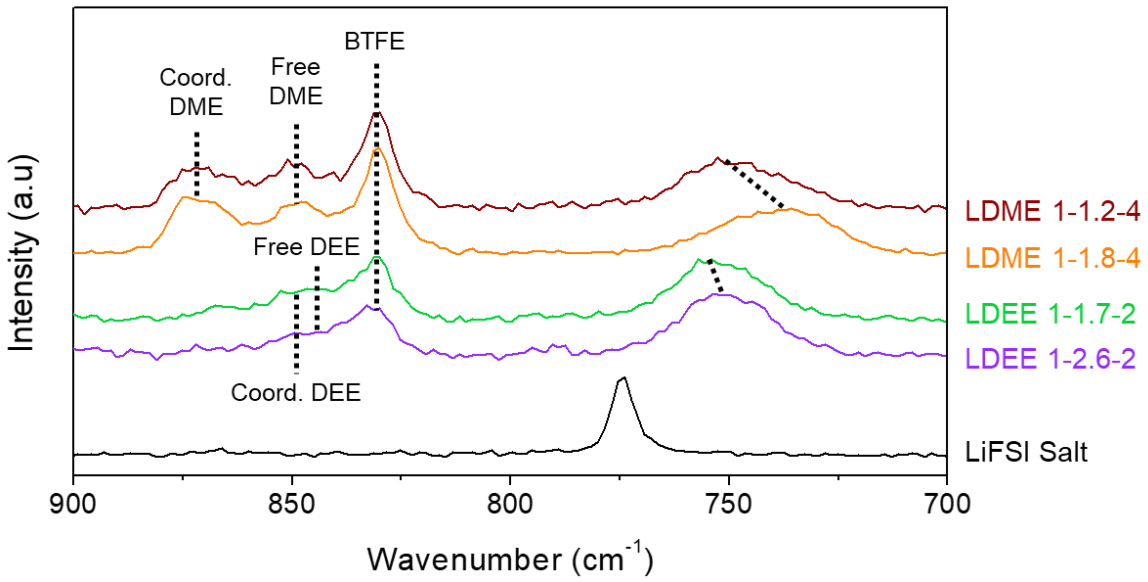

Figure S17. Measured Raman of electrolytes of interest. The S-N-S bending mode shown in the LiFSI salt spectra represents the greatest degree of ion-pairing found in the solid phase. Assignments for the solvent peaks can be found in our previous works.[12,13]

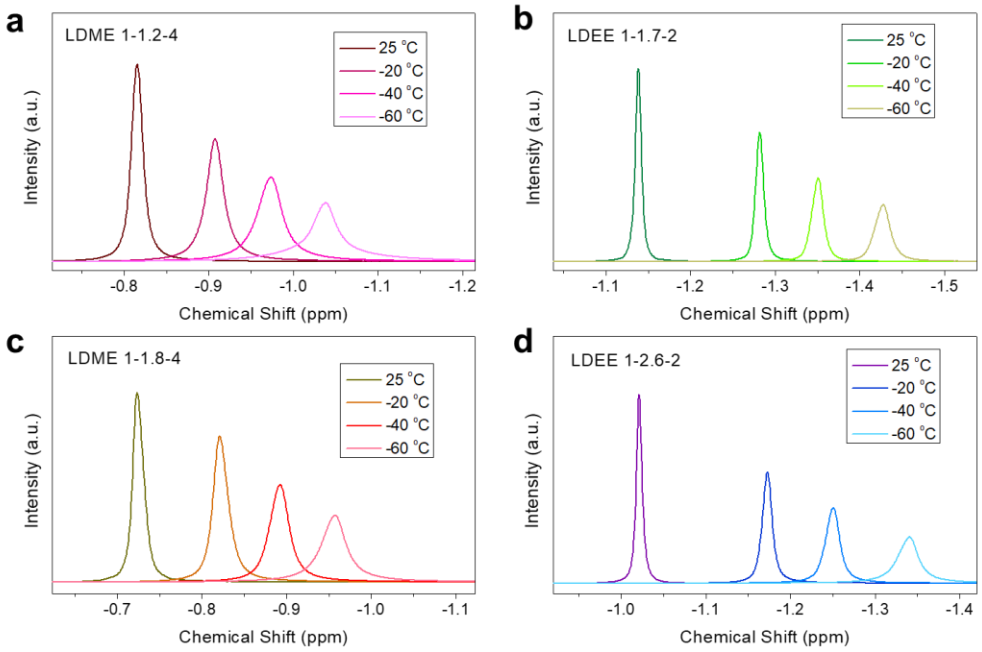

Figure S18. Measured ^{7}Li NMR spectra of LHCE systems of interest as a function of temperature. All chemical shifts are relative to the 1 M LiCl D_2O reference at 23 ^{o}C.

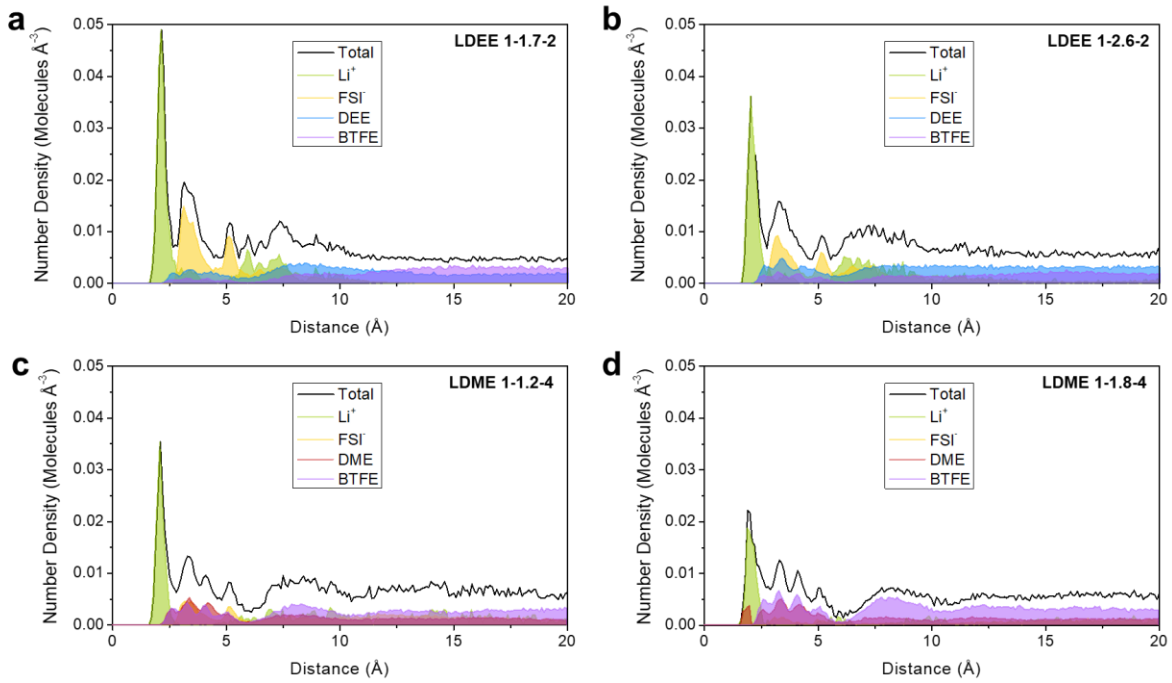

Figure S19. Electrolyte density profiles with respect to distance from the graphene electrode sampled from equilibration MD of the electrified interface. **a)** LDEE 1-1.7-2, **b)** LDEE 1-2.6-2, **c)** LDME 1-1.2-4, **d)** LDME 1-1.8-4.

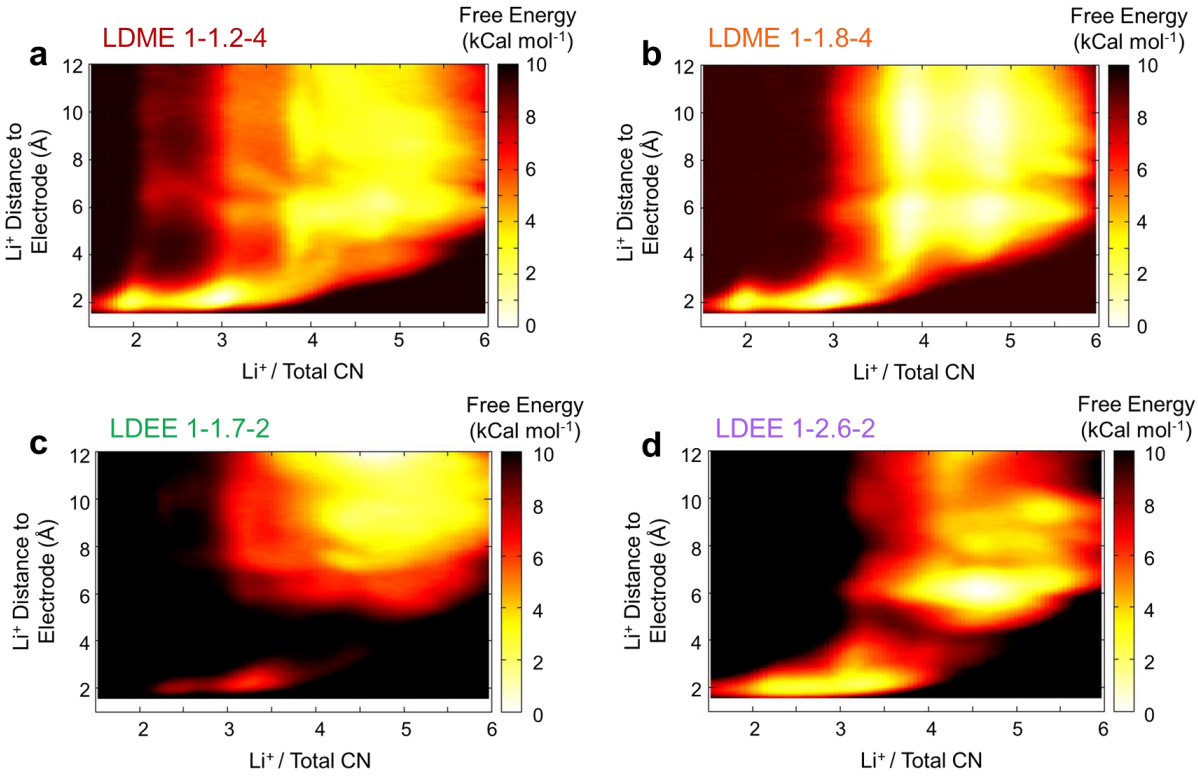

Figure S20. 2-D free energy spectra of **a)** LDME 1-1.2-4, **b)** LDME 1-1.8-4, **c)** LDEE 1-1.7-2, and **d)** LDEE 1-2.6-2 at the electrochemical interface with respect to Li^+/electrode distance and Li^+/total O coordination (solvating solvent + FSI^-).

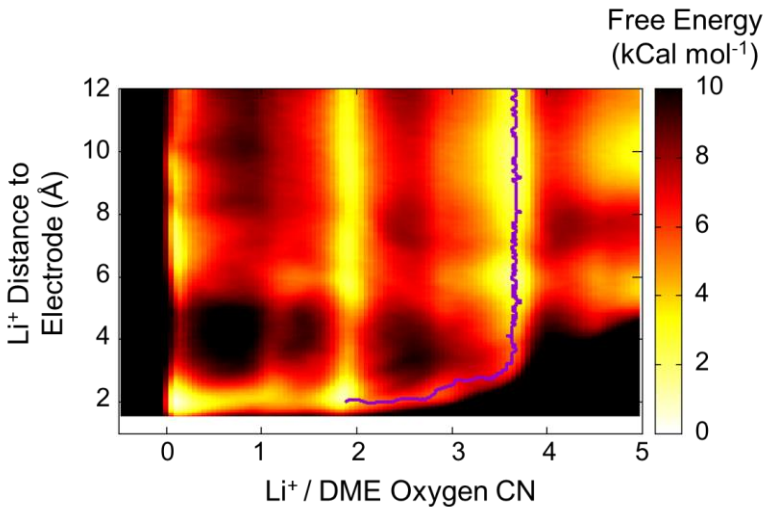

Figure S21. Depiction of the desolvation pathway of the DME CN = 2 state shown in Figure 4g.

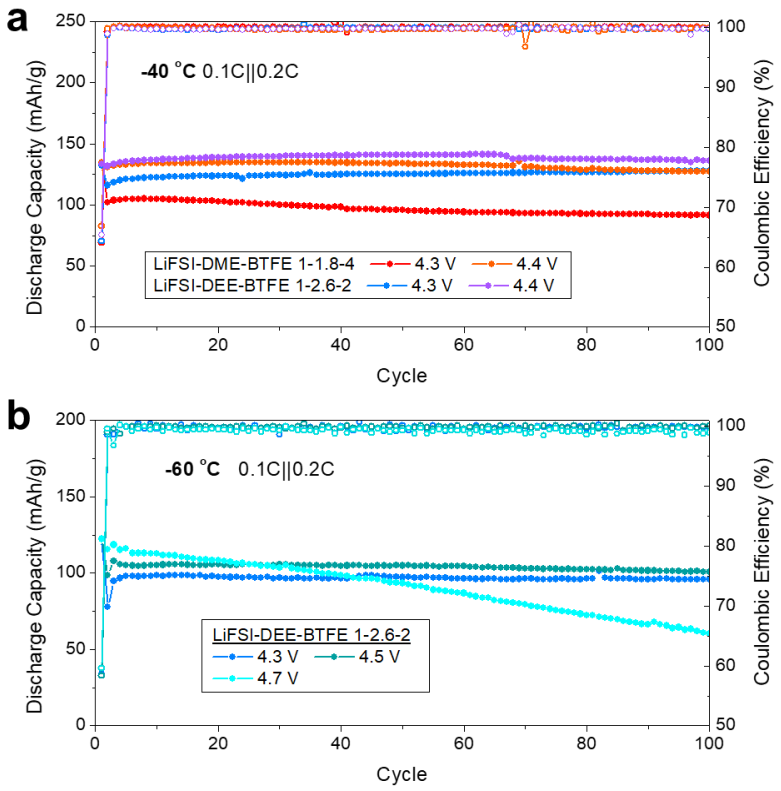

Figure S22. Low-temperature cycling of 10 mg cm^{-2} NCA ||20 µm Li coin-type full cells at various cutoff voltages. **a)** -40 ºC using LDME 1-1.8-4 and LDEE 1-2.6-2, **b)** -60 ºC LDEE 1-2.6-2.

a

Cycling Temperature	Capacity Retention	Average $V_{Discharge}$
23 °C	-	3.79 V
-20 °C	85.1 %	3.71 V
-40 °C	77.6 %	3.55 V
-60 °C	65.4 %	3.33 V

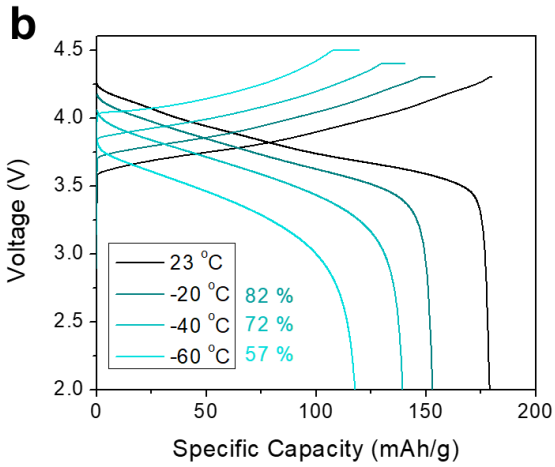

Figure S23. Energy retention of NCA || 20 µm Li pouch cells with 3 g Ah^{-1} electrolyte energy retention at reduced temperature. **a)** Tabulated capacity retention and average discharge voltage from **b)** voltage profiles from pouch cell with energy retention values at each temperature.

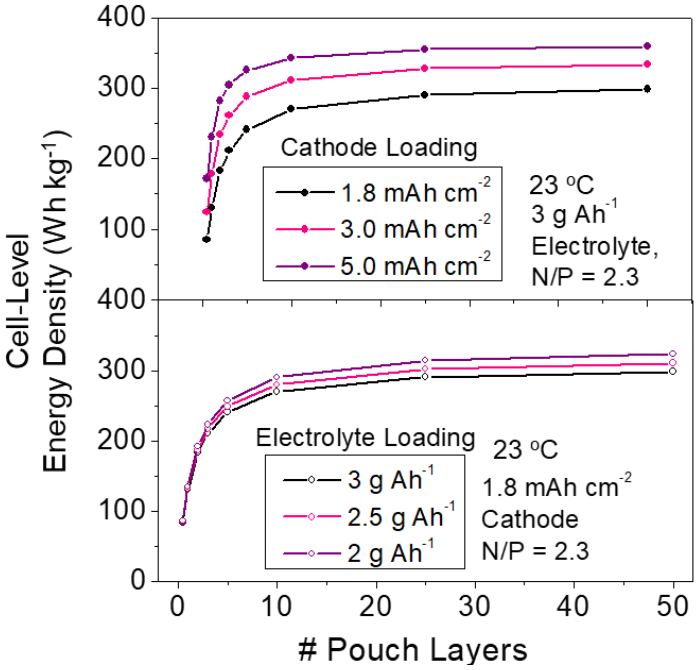

Figure S24. Dependence of projected energy density on number of double-sided pouch layers, cathode, and electrolyte loading.

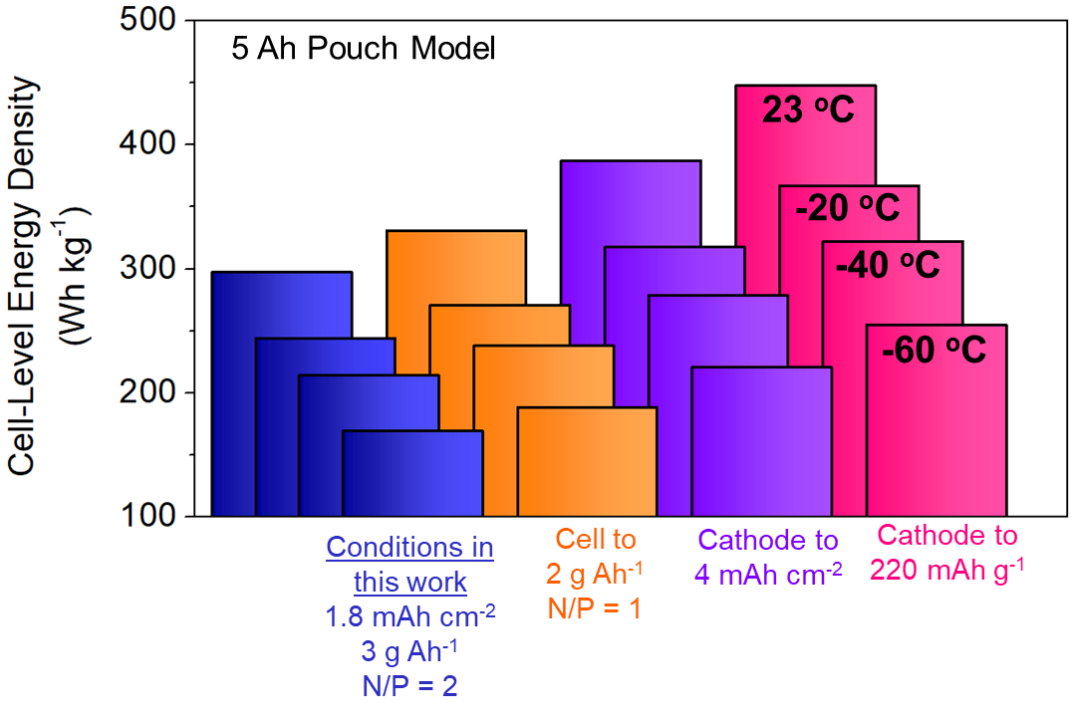

Figure S25. Cell engineering factors necessary for ultra-high energy density Li metal cells cycled at low-temperatures. Projected energy densities are based on the projected cell-level energy density model described in the methods section, with low-temperature energy densities calculated directly from the energy retentions shown in Figure S23. Doing so implies a generic performance fade acts on cells designed for room-temperature operation.

References

[1] Aurbach, D.; Youngman, O.; Gofer, Y.; Meitav, A. The Electrochemical Behaviour of 1,3-Dioxolane—LiClO4 Solutions—I. Uncontaminated Solutions. *Electrochimica Acta* **1990**, *35* (3), 625–638.

[2] Adams, B. D.; Zheng, J.; Ren, X.; Xu, W.; Zhang, J.-G. Accurate Determination of Coulombic Efficiency for Lithium Metal Anodes and Lithium Metal Batteries. *Adv. Energy Mater.* **2018**, *8* (7), 1702097.

[3] Wang, H.; Huang, W.; Yu, Z.; Huang, W.; Xu, R.; Zhang, Z.; Bao, Z.; Cui, Y. Efficient Lithium Metal Cycling over a Wide Range of Pressures from an Anion-Derived Solid-Electrolyte Interphase Framework. *ACS Energy Lett.* **2021**, *6* (2), 816–825.

[4] Hockney, R. W. *Computer Simulation Using Particles*; Hilger, 1988.

[5] Reed, S. K.; Lanning, O. J.; Madden, P. A. Electrochemical Interface between an Ionic Liquid and a Model Metallic Electrode. *J. Chem. Phys.* **2007**, *126* (8), 084704.

[6] Tuckerman, M. E.; Alejandre, J.; López-Rendón, R.; Jochim, A. L.; Martyna, G. J., A Liouville-operator derived measure-preserving integrator for molecular dynamics simulations in the isothermal–isobaric ensemble. J. Phys. A: Math. Gen. 2006, 39 (19), 5629

[7] Barducci, A.; Bonomi, M.; Parrinello, M. Metadynamics. WIREs Comput. Mol. Sci. 2011, 1 (5), 826–843.

[8] Fiorin, G.; Klein, M. L.; Hénin, J. Using Collective Variables to Drive Molecular Dynamics Simulations. Mol. Phys. 2013, 111 (22–23), 3345–3362.

[9] Baskin, A.; Prendergast, D. "Ion Solvation Spectra": Free Energy Analysis of Solvation Structures of Multivalent Cations in Aprotic Solvents. J. Phys. Chem. Lett. 2019, 10 (17), 4920–4928.

[10] Holoubek, J.; Baskin, A.; Lawson, J. W.; Khemchandani, H.; Pascal, T. A.; Liu, P.; Chen, Z. Predicting the Ion Desolvation Pathway of Lithium Electrolytes and Their Dependence on Chemistry and Temperature. J. Phys. Chem. Lett. 2022, 4426–4433.

[11] Barducci, A.; Bussi, G.; Parrinello, M. Well-Tempered Metadynamics: A Smoothly Converging and Tunable Free-Energy Method. Phys. Rev. Lett. 2008, 100 (2), 020603.

[12] Holoubek, J.; Kim, K.; Yin, Y.; Wu, Z.; Liu, H.; Li, M.; Chen, A.; Gao, H.; Cai, G.; Pascal, T. A.; Liu, P.; Chen, Z. Electrolyte Design Implications of Ion-Pairing in Low-Temperature Li Metal Batteries. Energy Environ. Sci. 2022, 15 (4), 1647–1658.

[13] Holoubek, J.; Liu, H.; Wu, Z.; Yin, Y.; Xing, X.; Cai, G.; Yu, S.; Zhou, H.; Pascal, T. A.; Chen, Z.; Liu, P. Tailoring Electrolyte Solvation for Li Metal Batteries Cycled at Ultra-Low Temperature. Nature Energy 2021, 6 (3), 303–313.